Scilight

Advanced Chemical Process Analysis

https://www.sciltp.com/journals/acpa

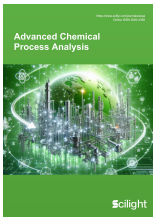

Article

On the Viscosity and Pipe Transport Behavior of Pure Ionic Liquids and Their Mixtures with Conventional Solvents

Victor Roberto Ferro [1,*], Jose-Luis Valverde [2], Raúl Collado [1], Juan de Riva [1] and José F. Palomar [1]

[1] Departamento Ingeniería Química, Universidad Autónoma de Madrid, 28049 Madrid, Spain
[2] Departamento de Ingeniería Química, Universidad de Castilla la Mancha, 13071 Ciudad Real, Spain
* Correspondence: victor.ferro@uam.es

How To Cite: Ferro, V.R.; Valverde, J.-L.; Collado, R.; et al. On the Viscosity and Pipe Transport Behavior of Pure Ionic Liquids and Their Mixtures with Conventional Solvents. *Advanced Chemical Process Analysis* **2025**, *1*(1), 5. https://doi.org/10.53941/acpa.2025.100005

Received: 14 July 2025
Revised: 2 September 2025
Accepted: 8 September 2025
Published: 16 September 2025

Abstract: This work addresses two interconnected topics: the viscosity-temperature behavior of ionic liquids and the techno-economic aspects of their pipe transport. A diverse selection of ionic liquids, conventional solvents, and their mixtures—covering a wide viscosity range—was analyzed under transport conditions representative of industrial processes. Based on an extensive experimental database compiled from the literature, new empirical correlations were developed to estimate the viscosity-temperature relationships of ionic liquids, using only their viscosities at 298.15 K. Rigorous simulations of pipe transport were conducted using the Pipe Segment model in Aspen HYSYS. A continuous transition in transport behavior was observed, ranging from highly viscous ionic liquids to low-viscosity solvents and their mixtures. This observation enables the use of heuristics developed for conventional fluids in the design of transport operations involving ionic liquids, provided that their specific characteristics are appropriately considered. Under the conditions and economic scenarios analyzed, the most cost-effective strategy for transporting viscous fluids involves using pipes with the largest feasible internal diameter, regardless of whether they are constructed from carbon steel or stainless steel. The use of conventional solvents as viscosity reducers does not appear to be economically viable, except when they are already present as impurities in the ionic liquid following purification. This may, additionally, reduce the cost associated with ionic liquid recovery. Leveraging heat integration instead of relying on external heating fluids for the thermal conditioning of ionic liquids can reduce transport costs by enabling operation at higher temperatures, which increases fluid velocity without exceeding the pressure drop limit.

Keywords: ionic liquids; solvent mixtures; viscosity; fluid transport; process modeling

1. Introduction

Ionic liquids (ILs), known for their exceptional physical properties [1], are widely recognized as promising alternative solvents to replace conventional volatile organic compounds in industrial applications such as separation processes, reaction media, and other related uses [2]. However, before this potential can be fully realized, several economic and technological challenges must be addressed. One of the most significant limitations is the high viscosity exhibited by many ILs [3,4]. This elevated viscosity often hinders mass and heat transfer in process operations involving ILs [5–8] and poses difficulties for their transport through pipes under economically viable conditions. Consequently, transport operations are acknowledged to have a substantial impact on the overall cost of processes

involving ILs [5–8]. Thus, significant efforts are being made and notable successes have been achieved in the synthesis of low-viscosity ILs [9–11], as, for instance, the 1-butyl-1-methylpyrrolidinium thiocyanate ([bmim][SCN]) included in this work (Figure 1). Despite the successful development of ILs with low viscosities, it remains crucial to objectively assess the implications of high viscosities for their potential industrial applications.

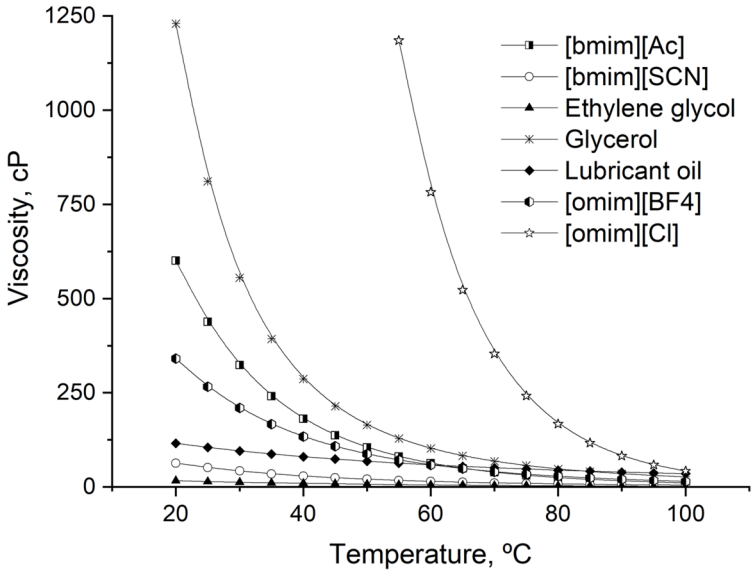

Figure 1. Temperature dependence of viscosity for selected pure ILs and conventional organic fluids used in industrial processes.

The solutions widely accepted for reducing the viscosity of ILs, and consequently considered in this work, are based on the well-established fact that their viscosities decrease exponentially with both the temperature (Figure 1) and the concentration of conventional solvents and gases in the corresponding mixtures (Figure 2).

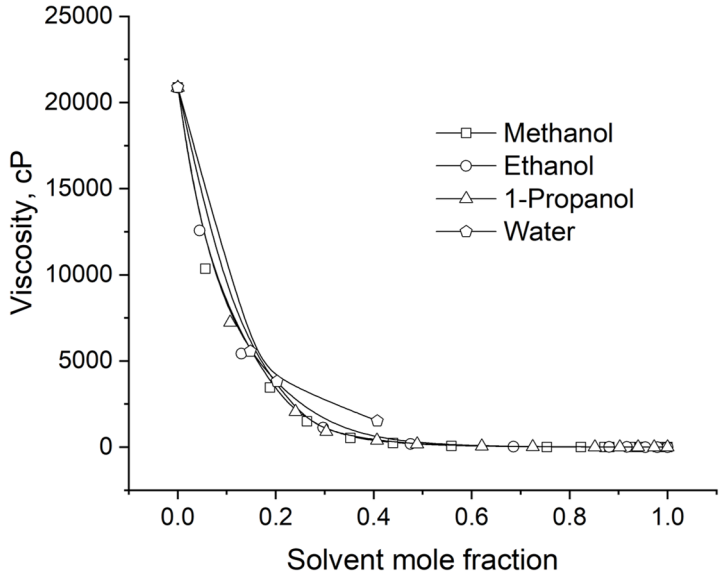

Figure 2. Effect of solvent molar fraction on the viscosity of (Solvent + [omim][Cl]) mixtures [12,13].

Any study on this topic requires extensive, high-quality data on the viscosity of ILs and their related properties. However, obtaining such data through experimental techniques is challenging due to the following factors: (i) The unique characteristics of ILs, such as high viscosity and low vapor pressure, limit the applicability of traditional experimental methods, which were primarily developed for conventional solvents, and (ii) The vast number of potential ILs for each application, owing to their "designer solvent" nature [14,15] makes comprehensive experimental evaluation impractical. As a result, alternative theoretical and semi-empirical approaches [3] are essential for reliably estimating IL viscosity and assessing its influence on potential applications.

The problem outlined above becomes even more complex when considering that, in addition to data on the thermophysical, thermodynamic, and transport properties of pure ILs and their mixtures, information is also required on the technological, economic, and environmental performance (among other aspects) of the new technologies based on them. A potential solution to this challenge, at least in the early stages of developing new IL-based processes, lies in the use of process simulation [16].

This study addresses several distinct, yet interconnected aspects of the issue outlined in this Introduction:

1. Based on the experience gained in previous studies [17,18], this work investigates the relationship between viscosity at room temperature ($\eta^{298.15K}$) and the temperature-dependent parameter in Andrade's equation. The objective is to develop simple models capable of predicting the viscosity of any IL as a function of temperature, using minimal input data, whether obtained experimentally or through theoretical approaches.
2. The influence of temperature and the nature of pure ILs on their transport behavior is assessed using a multivariable nonlinear model, developed from data obtained through process simulations involving ILs and conventional solvents with markedly different viscosities.
3. Four-parameter mixing rules of the form ln(Viscosity/*cP*) = *f*(Temperature, Composition) are fitted to estimate the viscosities of (Solvent + IL) binary mixtures, with the aim of evaluating different strategies for reducing the viscosity of ILs specifically, by using conventional solvents as viscosity-reducing agents to enhance their transportability.
4. Finally, the pipe transportation of ILs is assessed. The pressure drops associated with the transport of pure ILs and their mixtures with conventional solvents are evaluated as a function of various factors, including fluid properties, transport conditions, flow velocity, temperature, and pipe dimensions. Sensitivity analyses and optimization exercises are conducted to identify the key factors influencing pressure drop during the pipe transport of pure ILs or their mixtures, with the objective of proposing technically and economically viable solutions for industrial-scale processes. To summarize the findings of this section, a rational interpretation of both the transport behavior of ILs and their mixtures, as well as the technical solutions proposed, is provided based on the predominant flow regime under different operating conditions.

2. Computational Details

The viscosity of the pure ILs. Andrade's equation [19], Equation (1), was selected to describe the temperature dependence of viscosity for pure ILs, as it is simpler than other models used for similar purposes [3], while still offering reasonably good predictive capability [17,18] for engineering purposes.

$$\ln\left({}^{\eta}/_{cP}\right) = A_1 + \frac{B_1}{T} \tag{1}$$

where: η is the viscosity (in *cP*). *T* is the absolute temperature (in K). A_1 and B_1 are adjustable parameters. Subscript 1 of these parameters refers to the equation number.

In the present work (Table 1), the number of pure ILs for which the parameters of Andrade's equation were obtained has been increased compared to the previous study [17], following the procedure described therein. Furthermore, in 24% of the ILs listed in Table 1 of the previous study, the regression was improved through the incorporation of new data.

Another reason for selecting Andrade's equation is its ability to provide a complete description of the $\eta = f(T)$ relationship for a pure component within the two-dimensional space defined by the adjustable parameters A_1 and B_1, as illustrated in Figure 3 of Reference [17].

To obtain the parameters of the equation $B_1 = f(\eta^{298.15K})$, the previously mentioned database was used and divided into two subsets: 80% for model training and the remaining 20% for validation. The ILs in the test set were selected to cover the full range of A_1 and B_1 values observed in the training set.

Viscosity of binary mixtures of ILs and conventional solvents. The four-parameter mixing rule, Equation (2), was applied to correlate the viscosity of binary liquid mixtures (Solvent + IL) with their compositions. This model accounts for both the temperature dependence of viscosity and the non-ideal behavior of the mixtures through the inclusion of quadratic and cross-interaction parameters.

$$\ln\left({}^{\eta_{Mix}}/_{cP}\right) = x_1 \cdot \ln\left({}^{\eta_1}/_{cP}\right) + x_2 \cdot \ln\left({}^{\eta_2}/_{cP}\right) + \left[\left(A_2 + \frac{B_2}{T}\right) \cdot x_1 \cdot x_2\right] + \left[\left(C_2 + \frac{D_2}{T}\right) \cdot x_1^2 \cdot x_2^2\right] \tag{2}$$

where: η_{Mix}, η_1 and η_2 are the viscosities (*cP*) of the mixture and the individual components 1 and 2, respectively. x_1 and x_2 are the mole fractions of both components in the binary mixtures. A_2, B_2, C_2 and D_2 are adjustable parameters. *T* is the absolute temperature. Hereafter, components 1 and 2 are the solvent and the IL, respectively. Subscripts of the adjustable parameters refer to the equation number.

Equation (2) is implemented in the Aspen Properties environment as the Andrade liquid mixture viscosity [20] being A_2, B_2, C_2 and D_2 the parameters *ANDKIJ/*1*, ANDKIJ/*2, *ANDMIJ/*1 and *ANDMIJ/*2, respectively, in the nomenclature of the Aspen Properties.

Individual viscosity versus composition data for several binary mixtures (Solvent + IL) were retrieved from the literature (https://ilthermo.boulder.nist.gov/, accessed on 15 November 2024) to determine the parameters of Equation (2) and to evaluate its predictive performance. Specifically, data for mixtures of methanol and water with 1-octyl-3-methylimidazolium chloride ([omim][Cl]) were obtained from references [12,13], respectively. The fitting of the experimental data to Equation (2), along with the corresponding statistical analysis (Table 1), was performed using a custom code developed in MS Excel-VBA. The quality of the regression was evaluated statistically using the Average Absolute Deviation (AAD, %) and the Relative Average Absolute Deviation (RAAD, %).

Table 1. Fitting of experimental data to Equations (1) and (2) and their statistical analysis.

Systems Evaluated	Experimental Conditions	Statistics of the Regressions
	Pure ILs	
395 pure ILs More than 9500 initial points	Usually, P = 1 atm From 5 to 30 temperatures for each IL	R^2 > 0.99 for all the ILs considered 22% of the initial points were discarded (see details below)
	(Solvent + IL) binary mixtures ($x_{Solv.}$ is the molar fraction of the conventional solvent in the mixture)	
99 (Solvent + IL) mixtures More than 650 data points	P = 1 atm; T constant (usually 298.15 K), $x_{Solv.}$ variable	R^2 > 0.98 for all the systems studied RAAD = 6.2%
8 (Solvent + IL) mixtures More than 50 data points	P = 1 atm T and $x_{Solv.}$ variables	R^2 > 0.97 for all the systems studied RAAD = 19.3%
(Methanol + [omim][Cl]) 45 data points	P = 1 atm 15 $x_{Solv.}$ and 3 temperature levels	R^2 = 0.9996; RAAD = 4.5% A_2 = 24.3727; B_2 = −8249.61; C_2 = −85.804; D_2 = 36,260.8
(Water + [omim][Cl]) 16 data points	P = 1 atm 4 $x_{Solv.}$ and 4 temperature levels	R^2 = 0.9916; RAAD = 6.4% A_2 = 24.5050; B_2 = −6826.17; C_2 = −45.313; D_2 = 12,176.1

As a rule, the fittings yield R^2 values greater than 0.99 and RAAD values below 10%, which can be considered reliable for property estimations during the initial stages of process engineering.

Validation of predictions and statistical analysis. As explained, experimental data on the viscosity of pure ILs and some of their mixtures with other solvents were obtained from the literature and the ILThermo database (https://ilthermo.boulder.nist.gov/, accessed on 15 November 2024) to fit the models considered in this work. A statistical procedure based on the confidence bands methodology was initially applied to refine the raw data, aiming to achieve the best possible model fitting. Further details on this statistical procedure can be found in references [17,18]. The Relative Absolute Average Deviation (RAAD), expressed as a percentage, was used to quantify the quality of the predictions and/or to compare two data series. The RAAD was calculated using Equation (3).

$$\mathrm{RAAD}(\%) = \frac{100}{n} \cdot \sum_{i=1}^{n} \frac{\left| X_i^{Calc.} - X_i^{Ref.} \right|}{X_i^{Ref.}} \tag{3}$$

where: X_i designates the variable to be compared; n is the number of data points. Superscript *Calc.* defines the calculated value for variable X and *Ref.* the value taken as reference in the statistical comparison.

Development of the property package for process simulation purposes. Process simulations were performed using Aspen HYSYS v14.5. The fluid package was first created in Aspen Plus and then transferred to Aspen HYSYS via the Export/Import functionalities available in both programs. Conventional solvents were selected from the APV140 PURE40 database included in Aspen Plus v14.5, while ILs were chosen from the ILUAM01 enterprise database [18]. The COSMO-SAC equation [21] of the COSMOSAC property model, as implemented in Aspen Properties, was used in all the simulations for estimating the thermodynamic properties of the fluids [18]. The viscosities of the pure ILs and their (Solvent + IL) mixtures were calculated using Equations (1) and (2), with parameters specified by the user, as is customary in the Aspen Properties environment. Density, viscosity, aggregation states, and other thermodynamic, thermophysical, and volumetric properties of the pure components and their mixtures, as obtained from the process simulator, were validated against experimental data to ensure the accuracy of the simulations. It was also confirmed that a homogeneous liquid phase was maintained in all fluid

transport scenarios explored in this work; that is, no liquid-liquid or vapor-liquid phase separation was observed under any of the conditions studied.

Modeling of transport operations. The transport of pure ILs, conventional solvents, and their mixtures through pipelines was assumed to follow the process flowsheet presented in Figure 3. Process simulations were conducted using the Aspen HYSYS model, also illustrated in Figure 3.

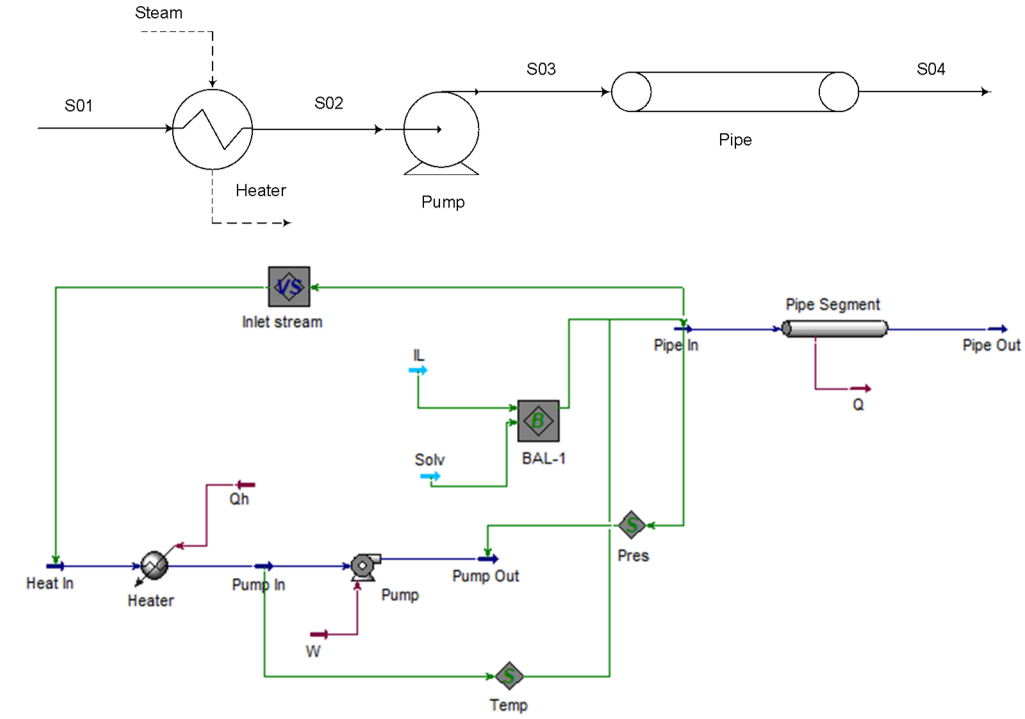

Figure 3. (**Up**): Process flowsheet of the transport operation studied in this work. (**Down**): Aspen HYSYS model used in calculations. Adjust operators used to fix design specifications have been omitted for clarity.

The Pipe Segment model available in Aspen HYSYS was used to simulate fluid transport. Only straight pipe sections were considered; fittings and bends were not included in the analysis. Fluid propulsion was simulated using the Centrifugal Pump model, also as implemented in Aspen HYSYS.

In pipe calculations, Beggs and Brill correlation [22,23] was used to predict pressure drops, as it accounts for both hydrostatic and frictional fluid losses across a wide range of flow conditions. This correlation includes corrections for frictional pressure drop in rough pipes and for liquid holdup in uphill and downhill flow scenarios [22]. According to Aspen HYSYS nomenclature, the "Pressure Drop Calculation" mode was employed. In this configuration, the fluid flow rate, pipe dimensions, heat transfer conditions, and outlet pressure ($P_{PipeOut}$) were specified. The program then calculates the pressure drop along the pipe segment ($\Delta P_{Pipe\ Segment}$) and, consequently, the initial pressure ($P_{Pipe\ In}$). To simulate fluid transport under atmospheric conditions $P_{S01} = P_{S04} = 1$ atm was specified. In this case, the relationship $P_{SO3} = P_{SO4} + \Delta P_{Pipe\ Segment}$ applies, meaning that the pump provides a pressure increase equal to the pressure drop across the pipe segment. If $P_{S01} < 1$ atm and $P_{S04} > 1$ atm, the pump must supply enough energy to overcome both the pressure difference $(P_{S04} - P_{S01})$ and the pressure drop in the line $(\Delta P_{Pipe\ Segment})$. The Heater model was included to simulate fluid heating and to analyze the effect of temperature on the transport operation. Pressure drop within the heater was neglected in the calculations. The Virtual Stream (*Inlet stream*) and Set (*Temp and Press*) operators, shown in Figure 3, were used to automatically transfer composition, mass flow, temperature, and pressure between the *PipeIn* and *HeatIn* streams, thereby avoiding consistency errors in the simulations. Due to limitations in Aspen HYSYS that prevent stream compositions from being selected as independent variables in automated computational procedures such as Case Studies, Adjust, and Optimizer, the Balance (BAL-1) manipulator was included in the process model. The mass flow of the *PipeIn* stream was fixed, and a component mole flow balance type was selected. Consequently, varying the mass flow of the *Solvent* stream was the adopted strategy to modify the feed composition to the process.

In general, the pressure drop was evaluated as a function of the following process variables:

1. The nature of IL. ILs with both different viscosities at room temperature and temperature-dependent viscosity decay rates were selected to explore distinct viscosity behaviors of the pure ILs and their mixtures with conventional solvents. Specifically, ILs were chosen based on the values of parameters A_1 and B_1 from

Andrade's equation, distributed along the B_1 vs. A_1 line shown in Figure 4 of this work, in good agreement with the previous findings of Ref. [17]. Namely, 1-octyl-3-methyl imidazolium chloride ([omim][Cl]), 1-bytyl-3-methyl imidazolium acetate ([bmim][Ac]), 1-octyl-3-methyl imidazolium tetrafluoroborate ([omim][BF_4]) and 1-butyl-3-methyl imidazolium thiocyanate ([bmim][SCN]) with viscosities (in cP) at 25 °C of approximately 20,000; 440; 255 and 50 were taken as reference systems.

2. Fluid temperature. Considering the exponential decay of viscosity with temperature in pure ILs and their mixtures with conventional solvents (Figure 1), a moderate temperature range (from 25 to 100 °C) was explored. This range is commonly used in industrial operations where viscous fluids must be transported through pipes [24–27].
3. The nature and concentration of the solvent in the binary mixture (Solvent + IL). Methanol and water were selected as conventional solvents and added in appropriate proportions relative to the IL [12,13] to achieve specific mixture behaviors under transport conditions (Figure 2).
4. Inside pipe diameter. Inside diameters within the range commonly used in industrial operations for transporting viscous fluids (203.4 to 304.8 mm) [24,25,27,28] were specified in the present simulations. Smaller diameters were also considered for cases involving low fluid flow rates.
5. Fluid velocity. Liquid velocities for the fluid transport in the interval between 0.5 and 1.5 m/s were evaluated in the present simulations. These velocities are also typical for transporting viscous fluids in industrial operations [25,28]. To define fluid velocity as a study variable, either the fluid flow rate or the pipe's internal diameter was specified as an independent variable, while the other ones were held constant (see further details in the description of the computational experiments below).

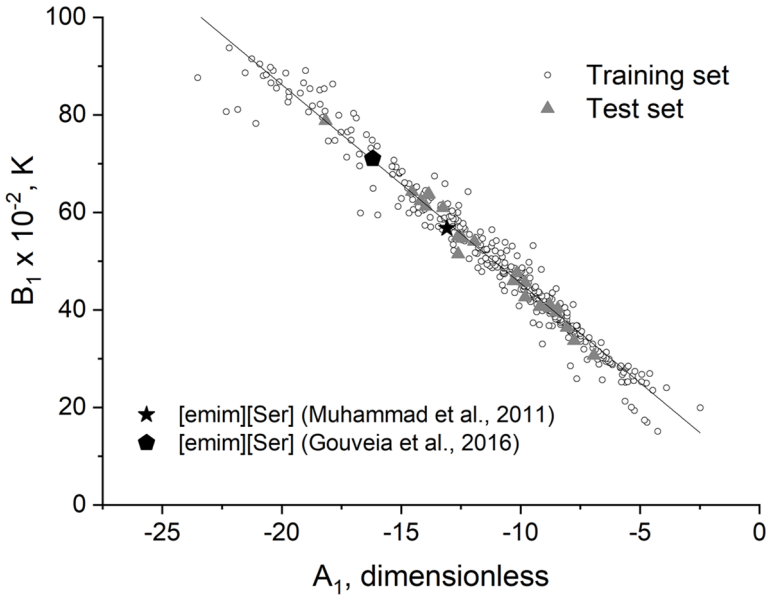

Figure 4. Relationship between the parameters A_1 and B_1 of the Andrade's equation, Equation (1), for the viscosity-to-temperature dependence in 393 different ILs [11,29].

In the simulations performed in this work, two key factors were considered as response functions, design specifications, or constraints in the corresponding computational exercises: pressure drop and fluid velocity. Pressure drops did not exceed 0.9 kPa/m, while fluid velocities remained below 2.0 m/s during the transport of viscous liquids through pipes [24–28]. To meet these two design specifications, the following variables were appropriately adjusted: fluid flow rate, temperature, and/or pipe inner diameter. In simulations of (Solvent + IL) binary mixtures transport, the solvent concentration was also treated as an independent variable. Design specifications, when required, were imposed using the Adjust operator available in Aspen HYSYS or incorporated into optimization calculations as constraints.

Experimental design. Two main computational experiments were conducted in this work. They were planned and executed using experimental design methodology, allowing for the extraction of maximum information from a minimum number of simulations [30,31].

Experiment 1. The effects of fluid nature, temperature, pipe inner diameter, and fluid velocity on pressure drops during the transport of pure ILs were evaluated. The fluid flow rate was adjusted to ensure the desired fluid velocity under the remaining specified transport conditions. The following rating/sizing specifications were always

used in all the simulations carried out in the current experiment: pipe length = 1 m, elevation change = 0, material = mild steel. Furthermore, fluid transport through the pipe was considered adiabatic; that is, no heat exchange between the transported fluid and the surrounding environment was considered (Q = 0 kJ/h, Figure 3).

Due to the heterogeneous nature of the study variables selected for this first analysis, the Doehlert design [32] was chosen for its flexibility in accommodating different numbers of levels for each variable. The design matrix was constructed using coded factors, such that the variation intervals for the independent variables were bounded between –1 and +1 in all cases, with intermediate values represented by fractional levels. This approach allowed both discrete qualitative and continuous variables to be treated uniformly. Temperature (X_1), pipe inner diameter (X_2), fluid velocity (X_3) and IL nature (X_4) were the factors considered. Five, seven, seven and three levels were used for factors X_1, X_2, X_3 and X_4, respectively. [omim][Cl], [omim][BF_4] and [bmim][SCN] were the ILs selected (variable X_4). Additionally, pure conventional solvents were included. The calculated pressure drop (kPa/m) was the response variable analyzed in the present experiment. Three-factor experimental designs (X_1, X_2, and X_3) were also carried out for individual ILs and conventional solvents, following the same methodology. Table 2 presents the factor levels and corresponding values used in the experimental design. The complete design matrix is provided in Table S1, where the three-factor designs are delimited by dashed lines.

Experiment 2. The effects of temperature and solvent molar fraction in the (Solvent + IL) mixture on pressure drop were investigated. This study focused on [omim][Cl] due to its highly viscous nature, which represents a limiting case for IL transportability. Two widely used conventional solvents (water and methanol) were considered as potential viscosity-reducing agents [12,13]. A five-level experimental design (5^2 = 25 cases) was selected, considering the potential non-linear behavior of the effects under evaluation. The complete design matrix is presented in Table S2. As in the first experiment, coded variables were used both to construct the design matrix and to formulate the corresponding model. Temperatures (°C) and solvent mole fractions selected were, respectively: 25 and 0 (level −1); 40 and 0.1 (level −0.5); 55 and 0.2 (level 0); 70 and 0.3 (level +0.5); 85 and 0.4 (level +1). In this case, a different strategy was employed to design the experiment: the fluid flow rate (10 t/h) and the pipe's inner diameter (203.4 mm) were fixed. Consequently, the fluid velocity and pressure drops were considered as response variables.

Table 2. Factor levels and values used in the experimental design for studying the influence of transport conditions on pressure drop in pure ILs and conventional solvents.

Real Variables				Coded Variables			
***T*, °C**	***D*, mm**	***v*, m/s**	**IL Nature**	X_1	X_2	X_3	X_4
	304.8	1.50			0.866	0.816	
	279.4	1.33			0.577	0.612	
100	254.0	1.17		1.0	0.289	0.204	
80	228.6	1.00		0.5	0	0	
60	203.2	0.83	IL3	0	−0.289	−0.204	0.791
40	177.8	0.67	IL2	−0.5	−0.577	−0.612	0
20	152.4	0.50	IL1	−1.0	−0.866	−0.816	−0.791

X_1: Temperature; X_2: Inside pipe diameter; X_3: Fluid velocity; X_4: IL nature. IL1: [omim][Cl]; IL2: [omim][BF_4]; IL3: [bmim][SCN]. In some studies, conventional solvents were also included.

Multivariable model. The results of the experimental designs were fitted to a multivariable polynomial model that accounts for linear (X_i), quadratic (X_i^2), and second-order interaction ($X_i \cdot X_j$) effects, as described in Equation (4):

$$y = \beta_0 + \sum_{i=1}^{k} \beta_i \cdot X_i + \sum_{i=1}^{k} \sum_{j(j\neq i)=1}^{l} \beta_{ij} \cdot X_i \cdot X_j + \sum_{i=1}^{k} \beta_{ii} \cdot X_i^2 \quad (4)$$

where: y represents the predicted response (pressure drop); X_i and X_j are the coded independent variables and β are the regression coefficients. β_0 is the intercept; β_i, β_{ii}, and β_{ij} are, respectively, the coefficients for the linear, quadratic, and two-factor interaction effects.

The parameter fitting and statistical significance analysis of the model were carried out using a custom VBA-MS Excel code. The coefficients were optimized using the non-linear Marquardt-Levenberg algorithm [33]. An analysis of variance (ANOVA) was employed to assess the statistical significance of both the overall model and its individual coefficients [30,31]. The criteria adopted for significance were either $p_c < p_0 = 0.05$ (where p_c is the calculated probability and p_0 is the significance level of the statistical analysis) and/or $F_{\text{Calculated}} > F_{\text{Critical}}$ (F_{Critical} is obtained for a significance level of 0.05). Finally, the application computes the importance ranking (in percentage)

of each input factor in the multivariable model response (output) as the average of the values obtained using the procedures summarized by [34].

Flow regime studies. The flow regime was assessed under various transport conditions for pure ILs, conventional solvents, and their mixtures. To characterize it, the Reynolds number (*Re*), defined by Equation (5), was used:

$$Re = v \cdot D \cdot \frac{\rho}{\eta} \tag{5}$$

where: v (m/s) is the fluid velocity; D (m) is the inner pipe diameter. ρ (kg/m^3) and η (Pa.s ≡ kg/m·s) are the fluid mass density and the viscosity, respectively.

The flow regime was classified based on Reynolds number (*Re*) values, following conventional criteria: turbulent for Re > 4000, laminar for Re < 2100, and transitional for values in between.

Comparison with conventional solvents and organic fluids. In some cases, for comparison purposes, the viscosity and transport behavior of the ILs and their mixtures with conventional solvents were compared to those of fluids commonly used in industrial operations. This comparison served as a reference in discussions regarding the feasibility of transporting ILs through pipes on an industrial scale.

In process simulations, conventional components were sourced directly from the PURE40 database in Aspen Properties, which includes data compatible with the COSMOSAC property model. Among the conventional organic fluids, a mineral lubricant oil was included and represented in the simulations as a heavy petroleum fraction. This fraction was created using the assay laboratory data presented in Table S3. The resulting pseudo-components had normal boiling points ranging from 240 to 830 °C. In this case, the thermodynamic properties were calculated using the Peng-Robinson equation of state.

Selection of optimal transport conditions. Process optimizations were carried out to identify the most cost-effective conditions for transporting the IL [omim][Cl] through pipes, using methanol as a viscosity-reducing agent. This IL was selected, again, for the analysis due to its high viscosity at room temperature. The computations were supported by the process model shown in Figure 3 and utilized the Optimizer functionality accessible in Aspen HYSYS. In all cases, the Total Annual Cost (TAC) of the operation was used as the objective function to be minimized (see details below). The independent variables considered, along with their corresponding variation intervals, are presented in Table 3.

Table 3. Independent variables and their variation intervals were used in the optimization exercises conducted in this study to determine the most cost-effective conditions for IL transportation through pipes.

Independent Variable	Low Bond	High Bond
Temperature of the stream fed to the pipe (*S03*), °C	26.0	85.0
Pipe inside diameter, mm	76.2	304.8
Solvent mass percentage in the mixture fed to the pipe (*S*01) [(1)], w%	0.07	40

[(1)] These concentrations correspond to mass flows (kg/h) of methanol 0.1 and 422 (Stream *Solv*, Figure 3).

In the optimizations, the mass flow of stream *PipeIn* (*S*01*,* Figure 3) was always 10 t/h. The lower bound selected for the solvent mass percentage in the transported mixture allows the solvent to be considered an impurity, resulting in a mixture that behaves as a highly pure IL. The viscosity of this mixture is approximately 19,190 cP at 25 °C, which is very close to that of pure [omim][Cl] at the same temperature (~19,200 cP). This approach helps avoid convergence issues during the optimization calculations. The lower temperature bound was set to prevent undefined values in the cost calculations.

In all the calculations carried out in the present optimization exercises, the following variables and factors were maintained fixed: pipe length = 50 m; $P_{S01} = P_{S04}$ = 1 atm; external temperature = 25 °C; ambient medium = air; air velocity = 1 m/s. Heat exchange between the mixture and the environment through the pipe wall was taken into account to estimate the required insulation thickness (see details below). The insulation material used was polystyrene foam. The overall heat transfer coefficients were calculated by considering the thermal resistances of the pipe wall, the insulation layer, and both the internal and external media. The initial point for all the optimizations was the same: methanol mass flow = 422 kg/h (mole fraction 0.156); inside diameter of the pipe = 101.6 mm, and T_{PumpIn} = 55 °C. The next two restrictions were imposed: fluid velocity ≤ 2.0 m/s and pressure drop ≤ 0.9 kPa/m. Optimization tasks were performed using gradient-based algorithms, following the criteria outlined below: data model = original optimizer; three convergence schemes were tested: BOX, SQP, and Mixed; tolerance = 10^{-5}, maximum change by iteration = 0.3; shift A = shift B = 10^{-4} (for more details, see the help of Aspen

HYSYS v 14.5). Different solvent prices, heating media, and tube materials were specified (see paragraph Equipment sizing and economic evaluation).

Equipment sizing and economic evaluation. The pipe dimensions (Figure 3), specifically the length and diameter, were typically predefined as part of the experimental design, sensitivity analyses, and optimization tasks carried out in this study. Only in particular cases were these dimensions treated as response variables. Two materials (carbon steel and stainless steel S316) were evaluated for pipe construction, differing in market price. The centrifugal pump model (Figure 3) was used solely to perform mass and energy balances, as it is probably not the best choice for pumping viscous fluids [25,26,28]. An adiabatic pump efficiency of 75% was assumed in all cases. Shell and tube heat exchangers were selected for thermal conditioning of the fluids. The methodology used for equipment sizing and for determining the thickness of thermal insulation in fluid transport operations (Figure 3) is summarized in Table S4.

Economic analyses were conducted in terms of *TAC*, which was calculated using Equation (6).

$$\text{TAC} = 0.1 \cdot \text{Immobilized Capital} + \text{Operating Costs} \quad (6)$$

where the immobilized capital is expressed in k$ and the operating costs in k$/operational year (operational year = 8000 h). 0.1 is the amortization factor of the investment.

The cost elements considered in calculating the immobilized capital for the transport operations (Figure 3) included the pipe, pump, heat exchanger, and thermal insulator. In this case, equipment costs were estimated using cost-capacity equations integrated into the flowsheet model (Figure 3) via user-defined models (Table S5). This approach enabled the incorporation of economic calculations into the model's analysis tools, including sensitivity analysis and optimization.

The operating costs associated with the transport operations (Figure 3) included pumping power, steam used as a heating medium, and the conventional solvent added to reduce the viscosity of the IL. The cost of the IL itself was excluded from the analysis because it was assumed to remain constant across all scenarios. In contrast, various prices were assigned to the conventional solvent: 0, 5, 20, 50, and 100 $/t. These values are somewhat hypothetical and are intended to represent a range of potential viscosity-reducing solvents, such as methanol or water. A price of 0 $/t reflects a scenario in which the solvent is considered an impurity already present in the IL, thereby incurring no additional cost in the transport process. A heating cost of zero (Figure 3) was also assumed, instead of accounting for steam usage, to represent a situation in which the thermal conditioning of the IL is achieved through heat integration using hot process streams. Table S6 presents the methodologies and pricing assumptions applied in these calculations.

3. Results and Discussion

Viscosity of the pure ILs. Although most of the pure ILs selected for this study are significantly more viscous at room temperature than the conventional fluids used for comparison, their viscosities become comparable at moderate temperatures (60 °C ≤ T ≤ 100 °C), as shown in Figure 1. [omim][Cl] is a clear example of this behavior: at 20 °C, it is 279 and 26 times more viscous than lubricant oil and glycerol, respectively. However, at 100 °C, its viscosity is only 1.2 to 1.6 times higher than that of these fluids. This indicates that heating pure ILs can be an effective strategy to enhance their transportability. Therefore, understanding the temperature dependence of IL viscosity is essential for designing the necessary heating operations.

Figure 4 of the current work revisited Figure 3 of the previous one [17], where it was observed that the coefficients of the Andrade's equation (A_1 and B_1) are linearly dependent on each other for pure ILs as shown in Equation (7).

$$B_1 = a_7 \cdot A_1 + b_7 \quad (7)$$

where: A_1 and B_1 are the parameters of the Andrade's equation, Equation (1). a_7 and b_7 are the adjustable parameters of Equation (7). Subscript 7 corresponds to the equation number.

In addition, B_1 correlates linearly (Figure 5) with $\ln\left(\eta^{298.15K}/_{cP}\right)$ for the pure ILs according to Equation 8):

$$B_1 = a_8 \cdot \ln\left(\eta^{298.15}/_{cP}\right) + b_8 \quad (8)$$

where: B_1 is the temperature-dependent parameter of the Andrade's equation. a_8 and b_8 are the coefficients of Equation (8). Subscript 8 concerns the equation number.

Equation (8) is particularly useful because, for many ILs, the viscosity at 298.15 K is known, while data at other temperatures may be unavailable. By obtaining $\eta^{298.15K}$, either experimentally or computationally, it

becomes possible to predict the temperature dependence of viscosity by appropriately combining Equations (1), (7) and (8). Table 4 summarizes the values of the parameters a_7, b_7, a_8, and b_8 obtained in this work with the information retrieved from the training and test sets of ILs.

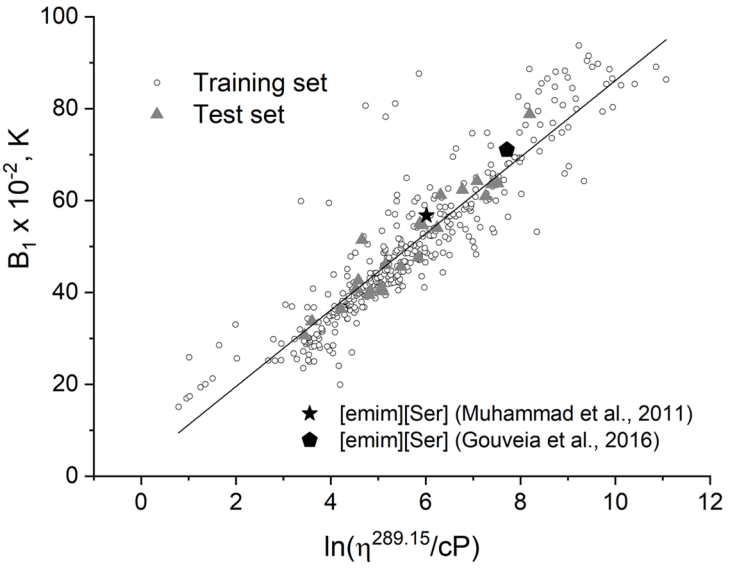

Figure 5. Relationship between the parameter B_1 of the Andrade's equation, Equation (1) and the $\ln\left(\eta^{298.15\mathrm{K}}{}^{2}/_{cP}\right)$ for the 393 ILs shown in Figure 3 [11,29].

Table 4. Adjustable parameters of Equations (7) and (8) proposed in this study for predicting the viscosity-temperature behavior of pure ILs.

Parameter	Training Set	(Training + Test) Set
	Equation (7)	
a_7	−407.861	−408.327
b_7	463.3405	457.002
R^2	0.9639	0.9644
	Equation (8)	
a_8	832.109	834.780
b_8	287.3712	276.250
R^2	0.8244	0.8273

The B_1 values obtained by fitting the viscosity-temperature data for each IL using Equation (1) were compared with those calculated from Equation (7), assuming that the A_1 values were those obtained from the regression to Equation (1). The relative average absolute deviation (RAAD) was 4.8% for the training set and 4.6% when both the training and test sets of ILs were considered together. In the RAAD calculations, Equation (3), $X^{Calc.}$ were the B_1 values obtained by Equation (7) and $X^{Ref.}$, the B_1 values obtained by fitting the η vs. T data for each IL according to Equation (1). Once again, the RAAD values obtained are acceptable for engineering calculations, particularly when applied to the conceptual and basic design stages of the processes.

As previously mentioned, Equations (7) and (8) can be used to predict the viscosity-temperature dependence of any IL, provided its viscosity at 298.15 K is known, either experimentally or computationally. This approach was applied to the 25 ILs selected as the test sample in this study. Using only the experimental viscosities at 298.15 K, the parameters A_1 and B_1 of Andrade's equation was estimated via Equations (7) and (8), and the complete $\eta = f(T)$ profiles were then generated using Equation (1). The calculated viscosities were statistically compared with experimental values in the $\ln\left(\eta/_{cP}\right)$ scale. For the complete dataset (25 ILs and 281 individual data points), an average RAAD of 7.0% was obtained using the parameters a_7, b_7, a_8 and b_8 derived from the training set. This value decreased to 6.8% when the adjustable parameters obtained from the combined training and test sets were used to compute the viscosities.

Figure 6, which illustrates the viscosity-temperature behavior for the [emim][Ser] IL, exemplifies the consistency of the computational methodology proposed herein, based on the integration of Equations (7) and (8). This IL has been the subject of two experimental studies [11,29] resulting in two distinct sets of viscosity-

temperature data (represented by filled points and solid lines in Figure 6). It is important to note that these datasets differ significantly, as acknowledged in reference [29]. A high RAAD = 22.7% was computed for the dataset published in [29] with respect to that reported by [11] in $ln(\eta/_{cP})$ scale. Additionally, in the present work, the individual $\eta^{298.15K}$ value along with the $\eta = f(T)$ dependency (represented also by filled points and solid lines in Figure 6) for the same IL were predicted by the QSPR model [35] implemented in the COSMOtherm v 20.0 program package [36].

Furthermore, the η-T behavior of the [emim][Ser] IL was calculated by combining Equations (7) and (8), using the $\eta^{298.15K}$ values corresponding to each data. The results are represented by open points and dashed lines in Figure 6. The computational procedure successfully reproduced the three individual data series with RAAD values (in %) of 3.4, 3.5, and 6.5 relative to [11,29] and QSPR [35] database, respectively. An additional dataset of $\eta = f(T)$ values (Figure 6) was generated by Equations (7) and (8), based on the viscosity at 298.15 K predicted by the neural network (NN) developed by [37].

In summary, Equations (7) and (8) can provide reliable predictions of the viscosity-temperature relationship for any IL, provided that the viscosity at 298.15 K is known. However, the accuracy of the $\eta^{298.15K}$ value is critical to ensuring the correctness of the predictions. Remarkably, the RAAD of the viscosities predicted in this work, when compared with the viscosity-temperature data used to obtain the $\eta^{298.15K}$ values, are lower than those calculated when comparing the two sets of experimental data reported by [11,29].

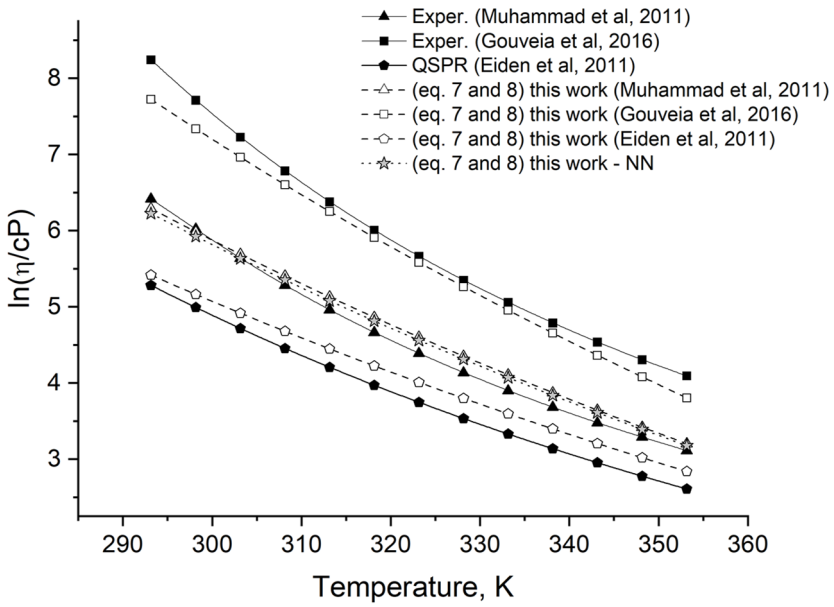

Figure 6. [emim][Ser] IL. Filled points and solid lines represent experimental viscosities reported by [11,29], as well as values computed using COSMOtherm with the QSPR model developed by [35]. Open points and dashed lines correspond to viscosities predicted by Equations (7) and (8) of this work, using the value of $\eta^{298.15K}$ for each individual data set. For the data set represented by stars, the value of $\eta^{298.15K}$ was obtained using a neural network developed by [37].

As expected, the (A_1, B_1) points obtained for the [emim][Ser] IL using Equations (7) and (8), based on different $\eta^{298.15K}$ values (Figure S1), lie on the regression line shown in Figure 4.

Pressure losses during pipe flow of pure ILs. Influencing factors. The pressure drops obtained from process simulations for the ILs and the transport conditions examined in the first experiment (Table S7) range from technically and economically unfeasible values ($\Delta P \approx 14$ kPa/m) to levels considered acceptable for industrial fluid transport ($\Delta P < 0.9$ kPa/m). As anticipated, pressure drops decrease with: (i) increasing temperature, (ii) increasing inner pipe diameter, (iii) decreasing flow velocity, and (iv) lower IL viscosity. Additionally, two-factor interactions significantly influence the pressure drop behavior during the transport of pure ILs.

The ANOVA analysis of the four-factor Doehlert design (Table 5) revealed a key finding: β_{14} was the unique significant coefficient of the polynomial multivariable model represented by Equation (4). The resulting model ($y = 1.738 \cdot X_1 \cdot X_4$) successfully explains 87% of the response variance. This indicates that temperature control plays a central and broadly effective role in ensuring the proper transport of any IL through pipes.

Moreover, the ANOVA analysis for the three-factor designs with individual ILs (Table 5) progressed stepwise from simpler models (as in the case of [omim][Cl]) to more complex ones (as for [bmim][SCN]). In all cases, the models were able to explain at least 95% of the response function. Interestingly, the lower the viscosity of the IL, the greater the influence of transport conditions (namely: inner pipe diameter and fluid velocity) on the pressure drop. In the case of [omim][Cl] (the most viscous among the ILs selected in this study) only the coefficient $\beta_1 = -6.439$ was found to be significant, indicating that temperature predominantly influences the pressure drop during transport operations. In contrast, for the least viscous IL selected, [bmim][SCN], all the coefficients in Equation (4) were found to be statistically significant. Remarkably, $\beta_3 = 0.070$ was the largest coefficient, suggesting that fluid velocity (X_3) is the primary factor affecting the pressure drop in this case, rather than temperature as observed with more viscous ILs. Intermediate behavior was observed for ILs with moderate viscosities at room temperature, such as [bmim][Ac] and [omim][BF_4].

The inclusion of conventional solvents in Table 5 (diethylene glycol and water) demonstrates the generality of the results and the conclusions from the previous paragraph regarding the transport of fluids with different viscosities. In the case of diethylene glycol, the pressure losses are described by a factorial model like that of [bmim][SCN], whose viscosities at 25 °C are comparable. Water, a low-viscosity fluid, represents a limiting case among the sample of fluids included in Table 5. In this case, the temperature-dependent terms in the factorial model are either not significant or have only a minor impact (for example, $\beta_1 = -0.003$) on the determination of pressure losses when compared to the other fluids considered. Indeed, the viscosity of water decreases by only a factor of 3.3 when the temperature increases from 25 °C to 100 °C. By contrast, all the coefficients associated with the transport operation terms are statistically significant.

Figure 7 shows the variation in the relative importance of the three factors considered (temperature, pipe inside diameter and fluid velocity) in determining the pressure drops associated with the transport of the selected fluids, ranging from the highly viscous [omim][Cl] to the low-viscous water, under the conditions of the first experiment (Tables 2 and S1) performed in this work. The results show that as fluid viscosity (at 25 °C) decreases, temperature plays a less significant role, while transport conditions, especially fluid velocity, become more influential.

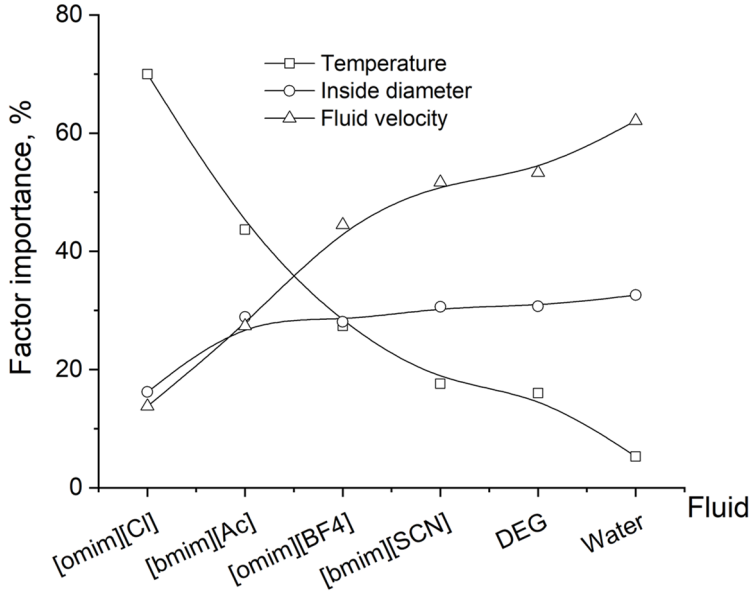

Figure 7. Relative importance of temperature, inner pipe diameter, and fluid velocity in determining pressure drops in Experiment 1, for both ILs and conventional solvents having a broad viscosity range at 25 °C (Table 5).

It is interesting to observe that the curves in Figure 7 evolve monotonically from highly viscous fluids to low-viscosity ones, without discontinuities when transitioning from ILs to conventional solvents. This suggests that, under similar conditions, pressure drop varies gradually with fluid viscosity, regardless of the fluid's nature. Consequently, the transport of ILs can be designed using the same heuristics developed for conventional industrial fluids, with appropriate adjustments to the factors that most significantly influence their transport behavior (see Table 5). In other words, the transport of pure ILs can be effectively designed to ensure pressure drops remain within technologically and economically viable ranges.

Table 5. Results of the ANOVA analysis for the Doehlert experimental design 1. Significant coefficients of the polynomial multivariable model represented by Equation (4) are shown. Factors: X_1 ≡ Temperature, X_2 ≡ Tube internal diameter; X_3 ≡ Fluid velocity, and X_4 ≡ IL nature. Conventional solvents (diethylene glycol and water) are included for comparison. Coded variables are used.

Four-Factors Design												
Multiple Correlation Coefficient			**Model (Significant Coefficients)**									
0.87			$\Delta P = 1.738 \cdot X_1 \cdot X_4$									
Three-Factors Designs												
$\Delta P = \beta_0 + \beta_1 \cdot X_1 + \beta_2 \cdot X_2 + \beta_3 \cdot X_3 + \beta_{12} \cdot X_1 \cdot X_2 + \beta_{13} \cdot X_1 \cdot X_3 + \beta_{23} \cdot X_2 \cdot X_3 + \beta_{11} \cdot X_1^2 + \beta_{22} \cdot X_2^2 + \beta_3 \cdot X_3^2$												
Fluid	$\eta_{IL}^{298.15K}$, cP	**Correlation Coefficient**	β_0	β_1	β_2	β_3	β_{12}	β_{13}	β_{23}	β_{11}	β_{22}	β_{33}
3-factors (X_1, X_2, X_3) design. X_4 ≡ [omim][Cl]	19,268	0.97		−6.439								
3-factors (X_1, X_2, X_3) design. X_4 ≡ [bmim][Ac]	439	0.95		−0.103								
3-factors (X_1, X_2, X_3) design. X_4 ≡ [omim][BF_4]	258	0.98		−0.057	−0.059	0.102						
3-factors (X_1, X_2, X_3) design. X_4 ≡ [bmim][SCN]	53	0.99	0.062	−0.024	−0.037	0.070	0.014	−0.022	−0.034	0.009	0.016	0.016
3-factors (X_1, X_2, X_3) design. Diethylene glycol	30	0.99	0.056	−0.020	−0.033	0.064	0.011	−0.017	−0.031	0.009	0.014	0.015
3-factors (X_1, X_2, X_3) design. Water	0.9	0.99	0.033	−0.003	−0.019	0.040			−0.019		0.007	0.011

The above is confirmed by the results shown in Figure 8, where the IL flow rate through the pipe segment was adjusted to meet the specified flow velocity. Additionally, either the fluid temperature or the pipe's inner diameter was modified to meet the design specification for pressure drop (≤0.9 kPa/m). Thus, the transport of [omim][Cl] requires temperatures ranging approximately between 40 °C and 70 °C, depending on both the inner pipe diameter and the fluid velocity. In contrast, the transport of ILs such as [bmim][Ac], [omim][BF_4], and [bmim][SCN] can be carried out at room temperature, if the pipe diameter and flow velocity are appropriately selected. Under the conditions explored in Figure 8, between 100 and 700 t/h of the ILs considered can be transported with pressure drops below 0.9 kPa/m.

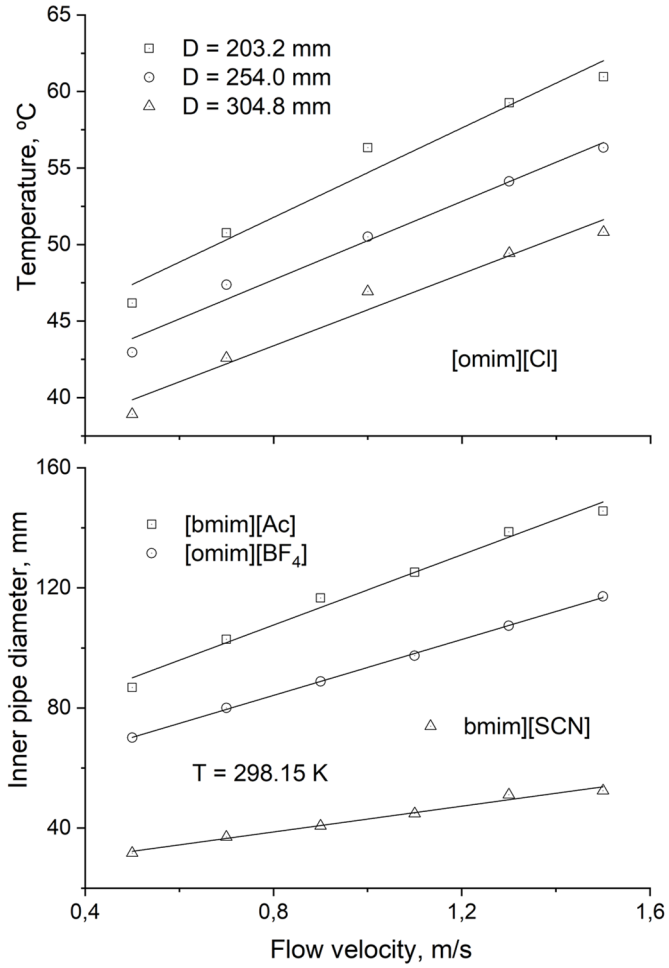

Figure 8. Conditions required to ensure pressure drops below 0.9 kPa/m during the transport of pure ILs through pipes. (**Top**): For [omim][Cl], representing a highly viscous IL at room temperature. (**Bottom**): For [bmim][Cl], [omim][BF_4], and [bmim][SCN], representing ILs with moderate to low viscosities at room temperature. In these calculations, the IL flow rate was adjusted to meet the specified flow velocity. Additionally, either the fluid temperature (**Top**) or the pipe's inner diameter (**Bottom**) was modified to satisfy the design specification for pressure drop.

The power required (Table 6) to transport the selected pure ILs through a 1 m of pipe with an inner diameter of 203.2 mm at a flow velocity of 1.5 m/s ranges from ~260 kJ/$t_{Transported}$ to ~1215 kJ/$t_{Transported}$. [omim][Cl] required an additional heating input of 7.56×10^4 kJ/$t_{Transported}$ to maintain a pressure drop of 0.9 kPa/m under the selected transport conditions. The calculated pressure drops ranged from 0.21 to 0.90 kPa/m. To provide a benchmark, the transport of conventional organic fluids was evaluated using the same operating conditions (Table 6). The power required correlates linearly with the pressure drop (Figure S2) across the entire set of fluids listed in Table 6, showing no discontinuities between ILs and conventional solvents.

Table 6. Energy requirements for the transport of selected ILs and conventional solvents. Pipe length: 1 m; fluid velocity: 1.5 m/s; pipe inside diameter: 203.2 mm. The fluid mass flow was adjusted to achieve the specified velocity. A maximum pressure drop of 0.9 kPa/m was set as the design criterion. If this condition was not met at 25 °C, the temperature was adjusted accordingly to satisfy the specification.

Fluid	Mass/Molar Flow Transported, $t \cdot h^{-1}/kmol \cdot h^{-1}$	Pressure Drops, kPa/m	Pumping Energy Consumes, $kJ/t_{Transported}$
[omim][Cl] (1)	173/749	0.90	1215
[omim][PF_6]	207/627	0.86	969
[hxmim][PF_6]	216/692	0.62	673
[bmim][Ac]	184/929	0.51	654
[omim][BF_4]	190/673	0.31	382
[bmim][PF_6]	227/799	0.27	280
Lubricant oil	155/418	0.18	272
[bmim][SCN]	184/934	0.21	264
Ethylene glycol	195/3145	0.19	224
Water	174/9672	0.09	0.12

(1) T = 60.1 °C and heating consumption = 7.56×10^4 $kJ/t_{Transported}$ are required to meet the design specifications.

Conventional solvents as viscosity-reducing agents in IL transport operations. For the temperatures and compositions of the mixtures (MeOH/H_2O + [omim][Cl]) explored in the second computational experiment (Table S2), the pressure drops ranged widely, from 0.08 to 12.6 kPa/m. Fluid velocities lay between 0.8 and 1.7 m/s, whereas the power required to overcome the pressure drops along the pipe varied from 3 to approximately 460 W. The complete set of results is reported in Table S8.

The factorial model obtained (Table 7) indicates that increasing both temperature and solvent concentration in the (MeOH/H_2O + IL) mixtures significantly reduce its viscosity (β_1 and $\beta_2 < 0$) as expected from the trends observed in Figure 2. Remarkably, the influence of temperature outweighs that of solvent concentration in both systems analyzed, i.e., $|\beta_1| > |\beta_2|$. In fact, temperature accounts for approximately 70% of the significance in determining the pressure drop in each system (Table 7). Moreover, the interaction effects between the two factors $(\beta_1 \cdot \beta_2)$ are also statistically significant. Finally, the quadratic effect of temperature is significant, whereas that of the solvent molar fraction is not.

Table 7. Polynomial two-factors model for the dependence $\eta = (T, x_{Solv})$ obtained in the second computational experiment accomplished in this work. Only significant coefficients are included. Coded factors are considered. X_1: temperature. X_2: solvent mole fraction.

Mixture	Statistical Validation	Significant Coefficients in Equation (4)	Importance T, %
(MeOH + [omim][Cl])	$R^2 = 0.903$ $F = 16.8 > F_{Critical.}$	$\Delta P = -1.9836 \cdot X_1 - 1.5185 \cdot X_2 + 2.6053 \cdot X_1 \cdot X_2 + 2.0151 \cdot X_1^2$	67.8
(H_2O + [omim][Cl])	$R^2 = 0.913$ $F = 19.0 > F_{Critical.}$	$\Delta P = -2.3192 \cdot X_1 - 1.2572 \cdot X_2 + 2.1969 \cdot X_1 \cdot X_2 + 2.3444 \cdot X_1^2$	72.9

It is noteworthy that the relative magnitudes of the model coefficients vary between the two solvents, suggesting that selecting the most effective viscosity-reducing agent for a specific application is not a straightforward task. The influence of solvent nature on the transport behavior of the mixture is also reflected in the importance of solvent concentration as a factor in determining the pressure drop. In the present case, this factor accounts for 32% when methanol is utilized as the viscosity-reducing agent, but only 27% when water is used.

Flow regime in the pipe transportation of pure ILs and their mixtures with conventional solvents. The *Re* number for selected pure ILs and conventional solvents, under the transport conditions (temperature, inner pipe diameter, and flow velocity) considered in the first experiment of this study, varied widely from approximately 15 to 45,200 (Figure 9), encompassing the entire range from laminar to turbulent flow regimes.

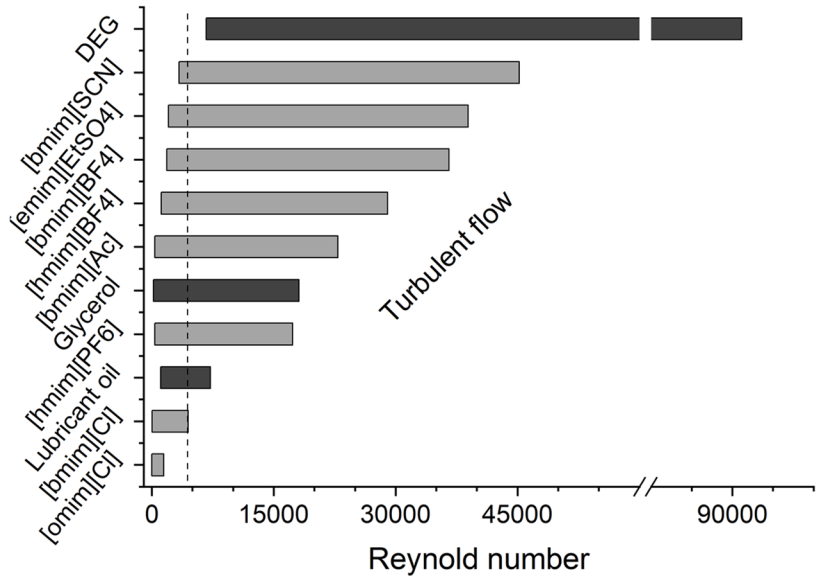

Figure 9. Reynolds number variation ranges for some ILs and conventional solvents considered in this work under the transport conditions defined in the three-factor design shown in Table S1. DEG: diethylene glycol. The dark gray bars represent conventional solvents.

Temperature was the primary factor influencing the Reynolds numbers (Table S9), showing a relative importance greater than 50% across all scenarios and fluids analyzed. As a rule, the Reynolds number increases exponentially with temperature when the remaining factors (inner pipe diameter and fluid velocity) are held constant. However, this behavior becomes quasi-linear for low-viscosity solvents such as water (Figure S3), which is consistent with the greater influence of operation-related factors over temperature (Table S9), representing in this case about 65% of the total contribution. It should be noted that the transition in this behavior from high-viscosity to low-viscosity fluids is gradual (Figure S4), with no qualitative distinction observed between ILs and conventional solvents.

The increase in temperature affects the ρ/η ratio in Equation 5, which exhibits behavior like that of the viscosity-temperature relationship (Figure 10).

Increasing the temperature from 20 to 100 °C results in a decrease in both the density and viscosity of the fluid. However, while the density decreases linearly with temperature, the viscosity exhibits an exponential decay. For the systems shown in Figure 10, the reduction in density at 100 °C compared to 20 °C is always less than 10%, whereas the viscosity decreases by 99%, 94%, 91%, 90%, and 69% for [omim][Cl], [omim][BF_4], [bmim][SCN], diethylene glycol, and water, respectively, over the same temperature range. These two effects together explain the behavior observed in Figure 10. It is important to highlight the gradual evolution of the ρ/η ratio with temperature, transitioning from high-viscosity fluids (such as [omim][Cl]) to low-viscosity ones (like water).

The continuous transition in transport behavior previously described for pure fluids (ILs and conventional solvents), from higher to lower viscosities, is also evident in their mixtures. As shown in Figure 11, the exponential increase in Reynolds' number with increasing temperature displays a similar profile throughout the transition from the pure IL to the pure solvent, including mixtures with compositions spanning the full range between these two extremes.

These results emphasize that transport behavior is mainly governed by the fluid's viscosity, regardless of its nature (whether it is an IL, a conventional solvent, or a mixture of both). In fact, for the mixtures and transport conditions analyzed in Figure 10, both $ln(\eta/_{cP})\ vs.\ T$ and $\ln(Re)$ vs. T exhibit linear trends ($R^2 > 0.99$ in all cases), with identical slopes but opposite signs (see Figure S5).

Optimization of the IL transporting by pipes. Despite the small deviations observed among the results obtained using the different optimization schemes applied in this study (Table S10), two distinct sets of conditions were identified that minimize the TAC for the transport of [omim][Cl]. For any conventional solvent price above \$0/t, the most cost-effective solution appears to involve using the largest available pipe diameter while minimizing the solvent concentration in the (MeOH + IL) mixture, that is, with the MeOH mass fraction approaching zero. This trend was observed regardless of the pipe construction material, whether carbon steel or stainless steel. Under these conditions, the maximum allowable pressure drop (0.9 kPa/m) is reached at liquid velocities below 0.1 m/s, and the TAC falls within the range of 10 to 40 k\$/year for the defined economic scenario (Tables S5 and S6).

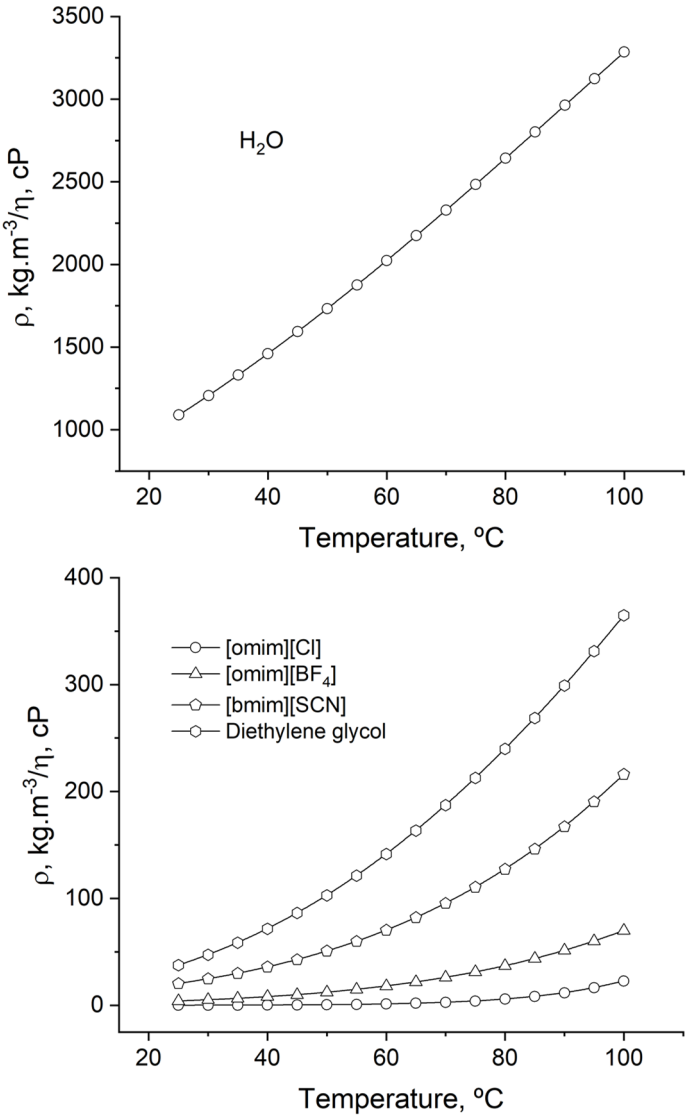

Figure 10. Dependence of the ρ/η ratio on temperature for various pure ILs and conventional solvents. Inner pipe diameter: 203.2 mm; fluid velocity: 1.0 m/s.

The preceding situation changes considerably when the viscosity-reducing solvent is assumed to have zero cost. In this case, the TAC of fluid transport is significantly lower (around 5 k$/year) for the conditions explored. This minimum is achieved by minimizing both the fluid temperature and the pipe's inner diameter, while maximizing the concentration of the conventional solvent in the IL mixture. As a result, the MeOH mass fraction reaches the maximum allowable value (Table 3) in the current design (40 w%). Interestingly, under these conditions, the pressure drop limit is maintained even at much higher fluid velocities (about 0.75 m/s) compared to the previous circumstances. As earlier discussed, this situation may correspond to a case in which the solvent is present as an impurity in the IL during the related purification operations, offering a dual economic benefit by simultaneously reducing both fluid transport costs and the expenses related to IL regeneration for recycling back into the process.

Utilizing the thermal energy of hot process streams enables cost reductions through all conditions considered in the optimization of IL transport (Table S10). Interestingly, in cases where the viscosity-reducing solvent has zero cost, the temperature that minimizes the TAC is the lowest possible (close to room temperature). However, for any other price of the conventional solvent, the optimal temperature increases to approximately 50 °C, which favors an increase in fluid velocity (from 0.07 to 0.21 m/s approximately) without exceeding the pressure drop limit (Table S10).

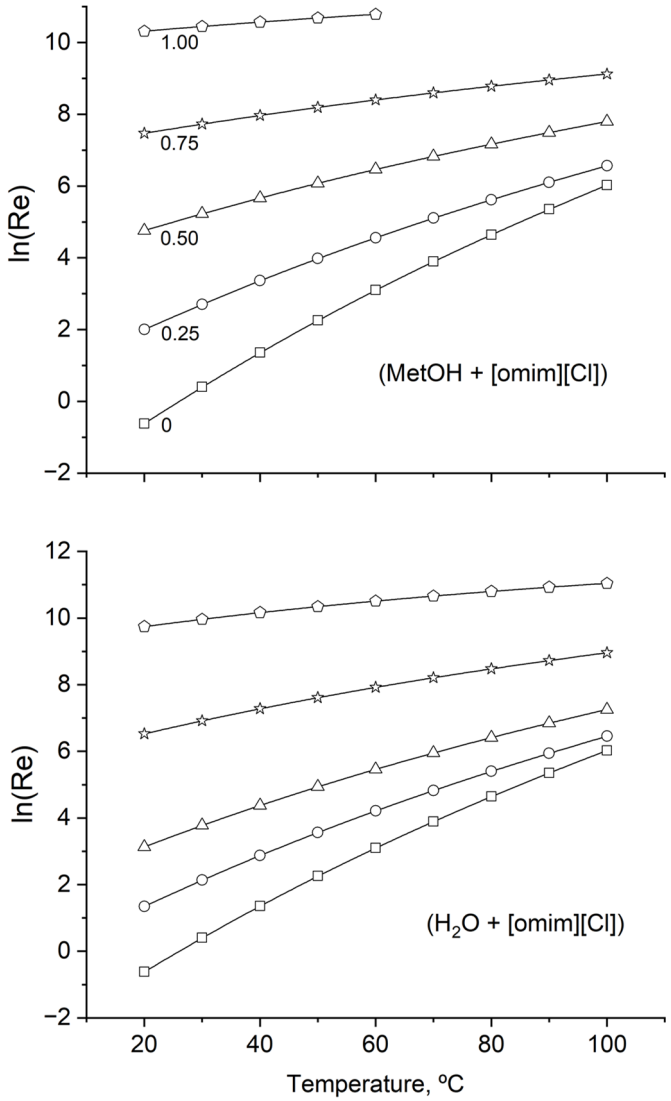

Figure 11. Behavior of the $\ln(Re) = f(T)$ dependence for mixtures of (MeOH/H_2O + [omim][Cl]) at different compositions. The numbers accompanying each curve indicate the molar fraction of MeOH/H_2O in the mixture. Operating conditions: mixture mass flow rate = 10 t/h, internal pipe diameter = 203.2 mm, pipe length = 1 m, adiabatic transport.

4. Concluding Remarks

- The temperature-dependent parameter of the Andrade's equation for pure ILs can be reliably estimated from the viscosity value at 25 °C using an empirical relationship, with the parameters determined in the present study. The accuracy of this prediction depends on the quality of the $\eta^{298.15\ \mathrm{K}}$ determination.
- The viscosity of binary (Solvent + IL) mixtures can be accurately predicted for engineering applications across wide temperature and composition ranges using four-parameter empirical mixing rules.
- The transport behavior of ILs evolves systematically from the most to the least viscous liquids (including conventional solvents and their mixtures) without any noticeable disruptions in performance. Therefore, the corresponding pipe transport operations can be designed using engineering heuristics derived from conventional fluids, while carefully considering the specific characteristics of ILs:
  - Temperature is the key process variable controlling the transportability of ILs through pipes, particularly in the case of highly viscous ILs.
  - As the viscosity at room temperature of the IL decreases, transport conditions become increasingly important in determining its transportability, making its behavior closer to that of conventional solvents.
  - When mixtures of ILs and conventional solvents are transported through pipes, both temperature and composition influence the transport process, with the relative importance of each factor depending on the nature of the components.

- The most cost-effective solution for transporting viscous ILs appears to be related to:
  - The use of pipes with the largest feasible inside diameter,
  - Utilizing the thermal energy of hot process streams to condition the IL, and/or
  - Transporting ILs containing low to moderate concentrations of conventional solvents as impurities, which could additionally reduce the cost of IL recovery operations.

Intentional dilution does not appear to be economically viable at any solvent price within the economic scenarios evaluated in this study.

Supplementary Materials

The additional data and information can be downloaded at: https://media.sciltp.com/articles/others/2509160918013932/ACPA-2508000023-Supplementary-Materials.pdf. Figure S1: Experimental and fitted values of the A_1 and B_1 parameters in Andrade's equation for the [emim][Ser] IL. Figure S2: Correlation between the pumping power required to move the fluid and the pressure drop in the pipe. Figure S3: Dependence of the Reynolds number on temperature for selected ILs and conventional solvents. Figure S4: Exponential dependence of the Reynolds number on temperature for various ILs and conventional solvents. Figure S5: Temperature dependence of ln(η/cP) and ln(Re) for an equimolar (H_2O + [omim][Cl]) mixture. Table S1: Doehlert design matrix for the study of influence of the transport conditions on the pressure drop for pure ILs and conventional solvents. Table S2: Design matrix ($5^2 = 25$ experiments) for the second computational experiment carried out in the current work. The effect of the temperature and the solvent mole fraction on the transport properties of the mixtures was studied. Table S3: Assay laboratory data used to create the petroleum fraction used to model the lubricant oil is considered a conventional fluid in this work. Table S4: Methodologies used in this work for the equipment´s sizing and determining the thickness of the thermal insulation used for reducing heat loss through the pipe wall in the fluid transport operations. Table S5: Procedures used to estimate the equipment costs. Table S6: Procedure and prices used to calculate the operating costs. Table S7: Results from the first experiment conducted in this study. Table S8: Results of the second computational experiment conducted in this study. Table S9: Importance of the factors considered in the three-factor design in determining the Reynolds number for several ILs and conventional solvents. Table S10: Results of the optimization exercises conducted under the conditions outlined in Table 3. References [38,39] are cited in Supplementary Materials.

Author Contributions

V.R.F.: conceptualization, methodology, software, original draft preparation; J.L.V.: data curation, software, validation, manuscript reviewing; R.C.: data curation, manuscript reviewing; J.d.R.: methodology, data curation, manuscript reviewing; J.F.P.: conceptualization, manuscript reviewing. All authors have read and agreed to the published version of the manuscript.

Funding

This research received no external funding.

Data Availability Statement

The data generated in this work are available in the Supplementary Material.

Conflicts of Interest

The authors declare no conflict of interest. Given the role as the Editor-in-Chief, Jose-Luis Valverde had no involvement in the peer review of this paper and had no access to information regarding its peer-review process. Full responsibility for the editorial process of this paper was delegated to another editor of the journal.

References

1. Singh, P.; Rajkhowa, S.; Sen, A.; et al. *Handbook of Ionic Liquids: Fundamentals, Applications, And sustainability*; John Wiley & Sons: Hoboken, NJ, USA, 2024. https://doi.org/10.1002/9783527839520.
2. Kalb, R.S. Commercial applications of ionic liquids. In *Toward Industrialization of Ionic Liquids*; Springer: Berlin/Heidelberg, Germany, 2020.
3. Gao, N.; Yang, Y.; Wang, Z.; et al. Viscosity of ionic liquids: Theories and models. *Chem. Rev.* **2023**, *124*, 27–123. https://doi.org/10.1021/acs.chemrev.3c00339.

4. Jiang, S.; Hu, Y.; Wang, Y.; et al. Viscosity of typical room-temperature ionic liquids: A critical review. *J. Phys. Chem. Ref. Data* **2019**, *48*, 033101. https://doi.org/10.1063/1.5090486.
5. Mota-Martinez, M.T.; Brandl, P.; Hallett, J.P.; et al. Challenges and for the utilisation of ionic liquids as solvents for CO_2 capture. *Mol. Syst. Des. Eng.* **2018**, *3*, 560–571. https://doi.org/10.1039/c8me00009c.
6. Hospital-Benito, D.; Lemus, J.; Moya, C.; et al. Process analysis overview of ionic liquids on CO_2 chemical capture. *Chem. Eng. J.* **2020**, *390*, 124509. https://doi.org/10.1016/j.cej.2020.124509.
7. Palomar, J.; Larriba, M.; Lemus, J.; et al. Demonstrating the key role of kinetics over thermodynamics in the selection of ionic liquids for CO_2 physical absorption. *Sep. Purif. Technol.* **2019**, *213*, 578–586. https://doi.org/10.1016/j.seppur.2018.12.059.
8. Mota-Martinez, M.T.; Hallett, J.P.; Mac Dowell, N. Solvent selection and design for CO_2 capture—How we might have been missing the point. *Sustain. Energy Fuels* **2017**, *1*, 2078–2090. https://doi.org/10.1039/c7se00404d.
9. Zhang, X.-M.; Huang, K.; Xia, S.; et al. Low-viscous fluorine-substituted phenolic ionic liquids with high performance for capture of CO_2. *Chem. Eng. J.* **2015**, *274*, 30–38. https://doi.org/10.1016/j.cej.2015.03.052.
10. Meindersma, G.W.; de Haan, A.B. Cyano-containing ionic liquids for the extraction of aromatic hydrocarbons from an aromatic/aliphatic mixture. *Sci. China-Chem.* **2012**, *55*, 1488–1499. https://doi.org/10.1007/s11426-012-4630-x.
11. Muhammad, N.; Man, Z.B.; Bustam, M.A.; et al. Synthesis and thermophysical properties of low viscosity amino acid-based ionic liquids. *J. Chem. Eng. Data* **2011**, *56*, 3157–3162. https://doi.org/10.1021/je2002368.
12. Gonzalez, E.J.; Alonso, L.; Dominguez, A. Physical properties of binary mixtures of the ionic liquid 1-methyl-3-octylimidazolium chloride with methanol, ethanol, and 1-propanol at T = (298.15, 313.15, and 328.15) K and at P = 0.1 MPa. *J. Chem. Eng. Data* **2006**, *51*, 1446–1452. https://doi.org/10.1021/je060123k.
13. Gomez, E.; Gonzalez, B.; Dominguez, A.; et al. Dynamic viscosities of a series of 1-alkyl-3-methylimidazolium chloride ionic liquids and their binary mixtures with water at several temperatures. *J. Chem. Eng. Data* **2006**, *51*, 696–701. https://doi.org/10.1021/je050460d.
14. Seddon, K. Ionic liquids: Designer solvents for green synthesis. *Chem. Eng.* **2002**, 33–35.
15. Freemantle, M. Designer solvents—Ionic liquids may boost clean technology development. *Chem. Eng. News* **1998**, *76*, 32–37. https://doi.org/10.1021/cen-v076n013.p032.
16. Palomar, J.; Lemus, J.; Navarro, P.; et al. Process simulation and optimization on ionic liquids. *Chem. Rev.* **2024**, *124*, 1649–1737. https://doi.org/10.1021/acs.chemrev.3c00512.
17. de Riva, J.; Ferro, V.R.; del Olmo, L.; et al. Statistical refinement and fitting of experimental viscosity-to-temperature data in ionic liquids. *Ind. Eng. Chem. Res.* **2014**, *53*, 10475–10484. https://doi.org/10.1021/ie5014426.
18. Ferro, V.R.; Moya, C.; Moreno, D.; et al. Enterprise ionic liquids database (ILUAM) for use in Aspen ONE programs suite with COSMO-based property methods. *Ind. Eng. Chem. Res.* **2018**, *57*, 980–989. https://doi.org/10.1021/acs.iecr.7b04031.
19. Andrade, E.N.C. The viscosity of liquids. *Nature* **1930**, *125*, 309–310.
20. Aspen Technology. *Aspen Plus (v 15.0) Help*; Aspen Technology Inc: Bedfordm, MA, USA, 2025.
21. Lin, S.T.; Sandler, S.I. A priori phase equilibrium prediction from a segment contribution solvation model. *Ind. Eng. Chem. Res.* **2002**, *41*, 899–913. https://doi.org/10.1021/ie001047w.
22. Payne, G.A.; Palmer, C.M.; Brill, J.P.; et al. Evaluation of inclined pipe, 2-phase liquid holdup and pressure loss correlations using experimental data. *J. Pet. Technol.* **1979**, *31*, 1198–1208.
23. Beggs, H.D.; Brill, J.P. Study of 2-phase flow in inclined pipes. *J. Pet. Technol.* **1973**, *25*, 607–617.
24. Ulrich, G.D.; Vasudevan, P.T. *Chemical Engineering Process Design and Economics: A Practical Guide*, 2nd, ed.; Process Publishing: Port Townsend, WA, USA, 2004.
25. Towler, G.; Sinnot, R. *Chemical Engineering Design: Principles, Practice and Economics of Plant and Process Design*; Elsevier: Boston, MA, USA, 2008.
26. Woods, D.R. *Rules of Thumb in Engineering Practice*; John Wiley & Sons: Hoboken, NJ, USA, 2008.
27. Turton, R.; Bailie, R.C.; Whiting, W.B.; et al. *Analysis, Synthesis and Design of Chemical Processes*; Prentice Hall: Upper Saddle River, NJ, USA, 2012.
28. Branan, C. *Rules of Thumb for Chemical Engineers*; Elsevier: Burlington, MA, USA, 2005.
29. Gouveia, A.S.L.; Tome, L.C.; Marrucho, I.M. Density, viscosity, and refractive index of ionic liquid mixtures containing cyano and amino acid-based anions. *J. Chem. Eng. Data* **2016**, *61*, 83–93. https://doi.org/10.1021/acs.jced.5b00242.
30. Lundstedt, T.; Seifert, E.; Abramo, L.; et al. Experimental design and optimization. *Chemom. Intell. Lab. Syst.* **1998**, *42*, 3–40. https://doi.org/10.1016/s0169-7439(98)00065-3.
31. Bezerra, M.A.; Santelli, R.E.; Oliveira, E.P.; et al. Response surface methodology (RSM) as a tool for optimization in analytical chemistry. *Talanta* **2008**, *76*, 965–977. https://doi.org/10.1016/j.talanta.2008.05.019.
32. Doehlert, D.H. Uniform shell designs. *J. R. Stat. Society. Ser. C* **1970**, *19*, 231–239.

33. Marquardt, D.W. An algorithm for least-squares estimation of nonlinear parameters. *J. Soc. Ind. Appl. Math.* **1963**, *11*, 431–441. https://doi.org/10.1137/0111030.
34. de Oña, J.; Garrido, C. Extracting the contribution of independent variables in neural network models: A new approach to handle instability. *Neural Comput. Appl.* **2014**, *25*, 859–869. https://doi.org/10.1007/s00521-014-1573-5.
35. Eiden, P.; Bulut, S.; Koechner, T.; et al. In silico predictions of the temperature-dependent viscosities and electrical conductivities of functionalized and nonfunctionalized ionic liquids. *J. Phys. Chem. B* **2011**, *115*, 300–309. https://doi.org/10.1021/jp108059x.
36. COSMOThermX, version 20.0.0, Revision 5273M; Dassault Systems: Waltham, MA, USA, 2019.
37. Omar Valderrama, J.; Makarena Munoz, J.; Erasmo Rojas, R. Viscosity of ionic liquids using the concept of mass connectivity and artificial neural networks. *Korean J. Chem. Eng.* **2011**, *28*, 1451–1457. https://doi.org/10.1007/s11814-010-0512-0.
38. Luyben, W.L. *Principles and Case Studies of Simultaneous Design*; John Wiley & Sons: Hoboken, NJ, USA, 2010.
39. Seider, W.D.; Seader, J.D.; Lewin, D.R. *Process Design & Principles: Synthesis, Analysis and Evaluation*, 2nd ed.; John Wiley & Sons, Inc.: New York, NY, USA, 1999.